Influence of collision energy on the $N(^2D)+O_2 \rightarrow O(^3P)+NO$ reaction dynamics: A quasiclassical trajectory study involving four potential energy surfaces

Irene Miquel, Jordi Hernando,[a] R. Sayós,[b] and Miguel González[c]
Departament de Química Física i Centre Especial de Recerca en Química Teòrica, Universitat de Barcelona, i Parc Cientific de Barcelona, C/Martí i Franquès, 1, 08028 Barcelona, Spain

(Received 4 April 2002; accepted 22 August 2003)

The influence of collision energy (E_T) on the dynamics of the $N(^2D)+O_2 \rightarrow O(^3P)+NO$ atmospheric reaction was studied by means of the quasiclassical trajectory method. The four lowest potential energy surfaces (PESs) involved in the process were used in the calculations ($2\,^2A'$, $3\,^2A'$, $1\,^2A''$, and $2\,^2A''$ PESs), and the nonadiabatic couplings between them were neglected. The dependence of the scalar and two-vector properties of the reaction with E_T was analyzed. Moreover, the different modes of reaction taking place were investigated. Although only one type of microscopic mechanism (abstraction) was found for the $2\,^2A'$, $3\,^2A'$, and $2\,^2A''$ PESs, two different modes of reaction (abstraction and insertion) were observed to coexist for the $1\,^2A''$ PES. For this PES, the abstraction mechanism is the most important one at room temperature, while the insertion mechanism increases its contribution to reactivity with E_T (it accounts for about half of the reactivity above 0.5 eV). © *2003 American Institute of Physics.* [DOI: 10.1063/1.1618221]

I. INTRODUCTION

The relevance of the study of the nitrogen atom in its first excited electronic state [$N(^2D)$] is due to the presence of this species in the earth-high atmosphere. Actually, its deactivation with ground-state molecular oxygen [$O_2(X\,^3\Sigma_g^-)$] could control the production of NO in the thermosphere and be an efficient source of highly vibrationally excited NO in the atmospheric region of 70–120 km.[1] Moreover, $N(^2D)$ plays an important role in photolysis systems, discharges in plasmas and chemical reactions.

The reaction between $N(^2D)$ and O_2 can take place through two reactive channels,[2,3]

$$N(^2D)+O_2(X\,^3\Sigma_g^-) \rightarrow O(^1D)+NO(X\,^2\Pi) \quad \Delta H^0_{298\,K} = -41.4 \text{ kcal mol}^{-1}, \tag{1}$$

$$N(^2D)+O_2(X\,^3\Sigma_g^-) \rightarrow O(^3P)+NO(X\,^2\Pi) \quad \Delta H^0_{298\,K} = -86.7 \text{ kcal mol}^{-1}. \tag{2}$$

Due to its interest, several experimental studies were devoted to the measurement of the global rate constant [including both reactive channels and $N(^2D)$ physical electronic quenching] of the $N(^2D)+O_2$ system.[4–14] The recommended value of the global rate constant at room temperature (298 K) is 5.2×10^{-12} cm^3 molecule^{-1} s^{-1}.[15] In addition, some experimental works determined the temperature dependence of the rate constant.[16,17] However, none of these measurements provided any information about the branching ratio of the two reactive channels of the $N(^2D)+O_2$ system. Concerning the dynamic properties of the process, only one experimental work was reported,[18] where the vibrational distribution for the NO product arising from the $N(^2D)+O_2$ reaction at 100 K was measured. The vibrational distribution obtained is inverted and peaked at $v'=7$.

From a theoretical point of view, a wealth of work was recently carried out in our group to investigate the $N(^2D)+O_2$ system. In Ref. 1 we showed that the rate constant for reaction (2) is several decades higher than the rate constant for reaction (1), so that the contribution of the latter process to the reactivity of the $N(^2D)+O_2$ system can be assumed to be negligible. This is due to the fact that the only potential energy surface (PES) that correlates reactants and products of reaction (1) has a very high energy barrier.[1] On the other hand, reaction (2) can take place through six PESs ($2\,^2A'$, $3\,^2A'$, $1\,^2A''$, $2\,^2A''$, $3\,^4A'$, and $3\,^4A''$), although only four of them ($2\,^2A'$, $3\,^2A'$, $1\,^2A''$, and $2\,^2A''$) present reaction barriers that are small enough to allow reactivity at low and moderate temperatures.[1] The contribution of the highly energetic $3\,^4A'$ and $3\,^4A''$ PESs can be ruled out.

In several recent works[1,19–23] we performed extensive *ab initio* studies on the most important PESs involved in reaction (2), using the complete active space self-consistent field/second-order perturbation theory on a CASSCF wave function (CASSCF/CASPT2) method. Afterwards, analytical functions describing satisfactorily the *ab initio* calculations of these PESs were derived and used to calculate the rate constant of reaction (2) over a wide range of temperatures employing the quasiclassical trajectory (QCT) and variational transition state theory (VTST) methods. A good agreement with the experimental values was obtained. The QCT vibrational distribution of NO was also computed for reaction (2) at 100 K and it was found to be more excited than the experimental one.

Other authors[24] recently performed *ab initio* calculations

[a]Present address: Applied Optics Group, Faculty of Applied Physics, University of Twente, P.O. Box 217, 7500 AE Enschede, The Netherlands.
[b]Electronic mail: r.sayos@ub.edu
[c]Author to whom correspondence should be addressed. Electronic mail: miguel.gonzalez@ub.edu

on some of the most important PESs for reaction (2) as well. They also carried out kinetic calculations on reaction (2) and computed the NO product vibrational distribution at 500 K by means of the QCT method. However, a thorough investigation of the dynamics of the title reaction has not been done yet.

The main purpose of this work is to employ the analytical representations of the PESs previously developed in our group to study theoretically the dynamics of reaction (2) by means of the QCT method, paying particular attention to the investigation of collision energy (E_T) on reactivity. The work is organized as follows: Section II deals with the PESs used and the computational method. Section III presents the results obtained and the discussion. The conclusions are given in Sec. IV.

II. COMPUTATIONAL METHOD

The four PESs used in this study were recently obtained in our group[19–23] by means of an extensive *ab initio* study based on the CASSCF (Refs. 25, 26) (17,12) calculations, where the standard correlation-consistent cc-pVTZ basis set of Dunning and co-workers[27] was employed. The treatment of the dynamic correlation was performed by means of the CASPT2 (Ref. 28) method using the G2 correction to the Fock matrix.

A many-body expansion[29] was used to obtain suitable analytical representations of the $2\,^2A'$,[19] $1\,^2A''$,[20] $3\,^2A'$,[21] and $2\,^2A''$ (Ref. 22) PESs of the title reaction. In all cases the minimum energy reaction path (MEP) involves an abstraction mechanism through a saddle point of bent geometry. The classical energy barriers associated to the saddle points are 0.19, 0.21, 4.60, and 7.51 kcal mol^{-1} for the $2\,^2A'$, $1\,^2A''$, $3\,^2A'$, and $2\,^2A''$ PESs, respectively. The corresponding NOO angles at the saddle points are 120.5°, 109.3°, 113.1°, and 115.6°, respectively. In the case of the $1\,^2A''$ PES an insertion mechanism evolving through a saddle point of C_{2v} geometry was also found. This saddle point has an ONO angle of 30.8° and a classical energy barrier of 1.43 kcal mol^{-1}.

To study the dynamics of reaction (2) on the four selected PESs, the QCT method[30,31] as implemented in the TRIQCT program[32] was employed, as we did in previous works from our group (see, e.g., Refs. 20, 33–37). Although the principles of this method were established long time ago, it can still be considered as the most useful theoretical tool to study the dynamics of chemical reactions. The accuracy of the numerical integration of Hamilton's differential equations was verified by checking the conservation of the total energy and total angular momentum for every trajectory, and performing back-integrations on some batches of trajectories. The integration step size chosen (5×10^{-17} s) was found to fulfill these conservation requirements for all calculated trajectories. The trajectories were started at an initial distance of 8 Å between the $N(^2D)$ atom and the center of mass of the O_2 molecule, thus ensuring that the interaction energy could be neglected with respect to the available energy of reactants. To study the reaction dynamics, the collision energy was fixed at different values (from 0.0388 eV to 1.00 eV), the vibrational level of the O_2 molecule was set at $v=0$ (99% of the molecules are placed in this level at 300 K), and the O_2 rotational distribution was sampled from the Maxwell–Boltzmann distribution at $T=300$ K. The final quantized vibrational distributions [i.e., $P(v')$] were obtained from vibrational radial action angle variables.[30]

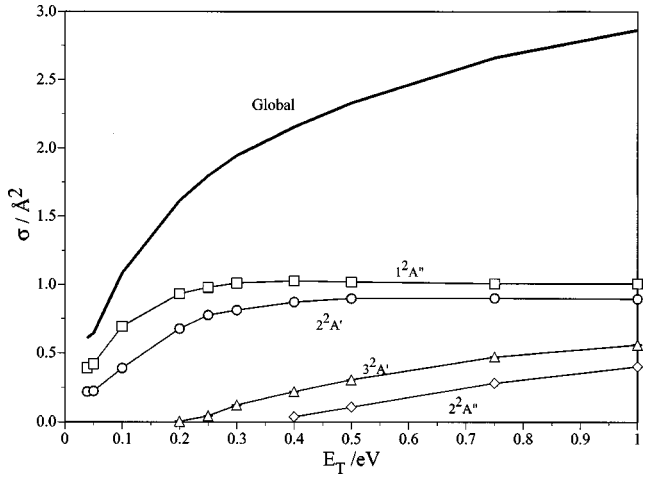

FIG. 1. Excitation function for the (○) $2\,^2A'$ PES, (□) $1\,^2A''$ PES, (△) $3\,^2A'$ PES, (◇) $2\,^2A''$ PES, and (—) global.

Four collision energies were considered in particular detail in the calculations: $E_T=0.0388$ (the average collision energy at 300 K), 0.25, 0.50, and 1.00 eV. Typically, for the computation of the cross section, batches of 15 000 trajectories were sampled for each collision energy and PES, while the calculation of product state distributions and two-vector properties for each E_T value required batches of 150 000 trajectories for each PES. The standard error (one standard deviation) was always kept below 5%.

III. RESULTS AND DISCUSSION

A. Scalar properties

Figure 1 shows the dependence of the cross section (σ) with E_T for each one of the PESs studied. To derive the σ values depicted in Fig. 1, the cross sections calculated by the QCT method on each PES were multiplied by 1/15 to take into account all the potential energy surfaces that correlate with reactants ($2\,^2A'$, $3\,^2A'$, $4\,^2A'$, $1\,^2A''$, $2\,^2A''$, $3\,^4A'$, $4\,^4A'$, $5\,^4A'$, $3\,^4A''$, and $4\,^4A''$). Figure 1 also shows the cross section of reaction (2) obtained as the sum of the contributions for the four main PESs involved in the reaction ($2\,^2A'$, $3\,^2A'$, $1\,^2A''$, and $2\,^2A''$).

The contribution of the $3\,^2A'$ and $2\,^2A''$ PESs to the cross section of reaction (2) is negligible for E_T values lower than 0.25 and 0.4 eV, respectively, due to their energy barriers. The threshold energies found for these two PESs are consistent with their energy barriers. As they present much lower energy barriers, the $2\,^2A'$ and $1\,^2A''$ PESs are reactive even for $E_T=0.0388$ eV. For all PESs σ increases with E_T until it reaches a plateau at sufficiently high energies, as expected for reactions with energy barrier along the MEP. The raise of σ with E_T is due to the increase of the reaction probability (P) with collision energy in all the PESs. With respect to the value of the maximum impact parameter

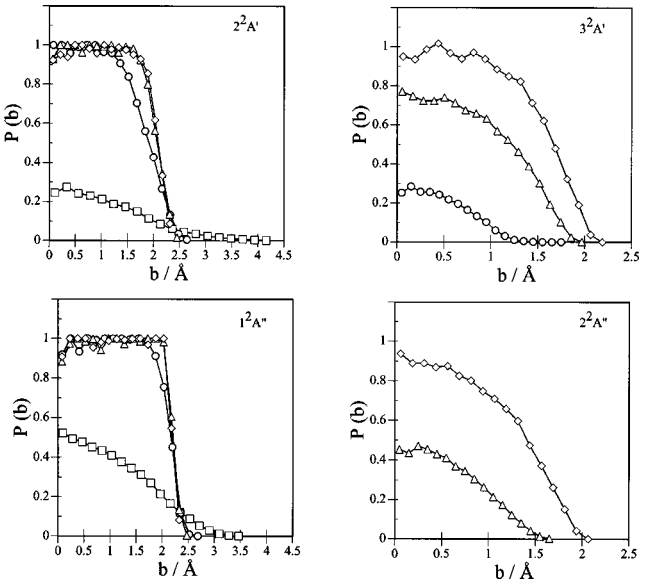

FIG. 2. Opacity function for the four PESs involved in reaction (2) at several collision energies: 0.0388 (□), 0.25 (○), 0.50 (△), and 1.00 (◇) eV.

($b_{\max}$), it only increases slightly with E_T for the $3\,^2A'$ and $2\,^2A''$ PESs, whereas for the more reactive $2\,^2A'$ and $1\,^2A''$ PESs $b_{\max}$ decreases significantly from 0.0388 to 0.25 eV and it remains constant for higher energies.

The opacity function [reaction probability, $P(b)$, vs the initial impact parameter (b)] presents a similar shape in all the PESs (Fig. 2). $P(b)$ is essentially constant between $b=0$ and some intermediate value of b, and after this it decreases progressively and reaches a value of zero at $b=b_{\max}$. When the value of the collision energy is close to the threshold energy of the PES, that is to say at 0.0388 eV for the $2\,^2A'$ and $1\,^2A''$ PESs, 0.25 eV for the $3\,^2A'$ PES and 0.5 eV for the $2\,^2A''$ PES, reactivity is more important at low values of b.

In Table I we show the average fractions of energy in products [$\langle f_i' \rangle$, $i=V$ (vibration), R (rotation), T (translation)] for the different PESs and the global reaction. For the overall reaction, the majority of the available energy (E_{av}) is channeled into NO vibrational energy and relative translational energy at $E_T=0.0388$ eV ($\langle f_V' \rangle=0.39$ and $\langle f_T' \rangle=0.40$), while a smaller fraction of E_{av} is channeled into NO rotation ($\langle f_R' \rangle=0.21$). As the collision energy increases, the average fraction of vibrational energy in products diminishes, which is accompanied by an increase in final translational energy ($\langle f_V' \rangle=0.26$ and $\langle f_T' \rangle=0.52$ at $E_T=1.00$ eV). The average fraction of NO rotational energy essentially remains constant at all collision energies. This behavior is consistent with the large exoergicity of the PESs, which leads to the existence of early saddle points. A similar trend is also observed for the $2\,^2A'$, $3\,^2A'$, and $2\,^2A''$ PESs, while in the case of the $1\,^2A''$ PES slight changes in $\langle f_V' \rangle$, $\langle f_R' \rangle$, and $\langle f_T' \rangle$ with E_T are found. This fact is due to the occurrence of different microscopic reaction mechanisms for the PESs, which will be further discussed in Sec. III C.

Changes in the energy distribution of NO with E_T are also evident from the evolution of the average NO vibrational level ($\langle v' \rangle$) (Table II) and NO vibrational distribution

TABLE I. Average energy fractions in products for the four PESs involved in reaction (2).

E_T/eV[a]	$2\,^2A'$	$3\,^2A'$	$1\,^2A''$	$2\,^2A''$	Global[b]
			$\langle f_V' \rangle$[c]		
0.0388	0.49		0.33		0.39
0.25	0.44	0.18	0.30		0.36
0.50	0.36	0.17	0.30	0.33	0.30
1.00	0.28	0.15	0.30	0.28	0.26
			$\langle f_R' \rangle$[c]		
0.0388	0.09		0.28		0.21
0.25	0.08	0.15	0.25		0.18
0.50	0.14	0.14	0.26	0.13	0.19
1.00	0.22	0.16	0.27	0.15	0.21
			$\langle f_T' \rangle$[c]		
0.0388	0.42		0.39		0.40
0.25	0.48	0.67	0.45		0.47
0.50	0.50	0.69	0.44	0.53	0.50
1.00	0.50	0.68	0.44	0.55	0.52

[a]The value of the available energy for the different values of the translational energy is 3.85, 4.06, 4.31, and 4.81 eV for $E_T=0.0388$, 0.25, 0.50, and 1.00 eV, respectively.

[b]The global average energy fractions were obtained according to the following expression: $\langle f_i' \rangle = [\sigma(2\,^2A')\langle f_i' \rangle(2\,^2A') + \sigma(3\,^2A')\langle f_i' \rangle(3\,^2A') + \sigma(1\,^2A'')\langle f_i' \rangle(1\,^2A'') + \sigma(2\,^2A'')\langle f_i' \rangle(2\,^2A'')] / [\sigma(2\,^2A') + \sigma(3\,^2A') + \sigma(1\,^2A'') + \sigma(2\,^2A'')]$.

[c]$\langle f_i' \rangle = E_i'/E_{\text{av}}$, where the available energy is given by $E_{\text{av}}=E_V'+E_R'+E_T'$, and E_V', E_R', and E_T' are the classical vibrational, rotational, and translational energies of products, respectively.

(Fig. 3). For the $2\,^2A'$, $3\,^2A'$, and $2\,^2A''$ PESs unimodal and inverted NO vibrational distributions are found for all E_T values explored. For these PESs the higher the collision energy is, the lower the peak of the distribution becomes. This trend is also observed for the global reaction. On the other hand, the vibrational distribution of the $1\,^2A''$ PES presents a bimodal feature that results from the overlap of an inverted distribution similar to that found for the other PESs and a less excited distribution peaked at low v' values. In this case, a slight increase of the average NO vibrational level with E_T is found. This behavior arises from the existence of two microscopic reaction mechanisms for the $1\,^2A''$ PES (cf. in Sec. III C). Hence, the vibrational distributions for the global reaction at $E_T=0.0388$ and 0.25 eV are bimodal as well.

B. Two-vector correlations

The analysis of the angular momentum transformation when the system evolves from reactants to products was per-

TABLE II. Average NO vibrational levels for the four PESs involved in reaction (2).

E_T/eV	$2\,^2A'$	$3\,^2A'$	$1\,^2A''$	$2\,^2A''$	Global[a]
0.0388	8.3		5.4		6.4
0.25	7.8	2.7	5.1		6.2
0.50	6.7	2.7	5.6	6.1	5.7
1.00	5.8	2.8	6.2	5.8	5.4

[a]The global average NO vibrational level has been obtained using an analogous expression to the one reported in Table I for the calculation of the global average energy fractions.

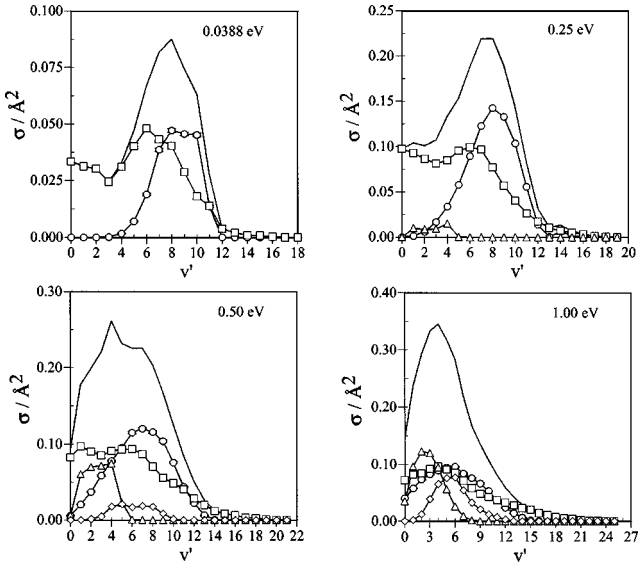

FIG. 3. Vibrational distribution of NO at several collision energies for the (○) 2 $^2A'$ PES, (□) 1 $^2A''$ PES, (△) 3 $^2A'$ PES, (◇) 2 $^2A''$ PES, and (—) global.

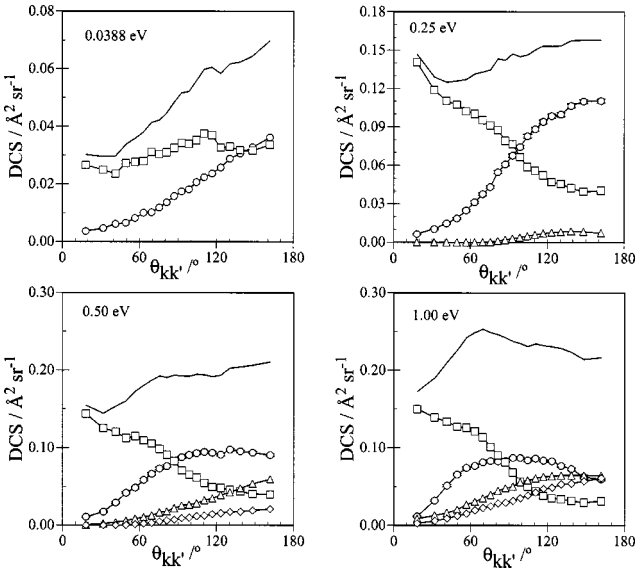

FIG. 4. DCS ($\mathbf{kk}'$) at several collision energies for the (○) 2 $^2A'$ PES, (□) 1 $^2A''$ PES, (△) 3 $^2A'$ PES, (◇) 2 $^2A''$ PES, and (—) global.

formed at all collision energies studied. Except for $E_T = 0.0388$ eV, the total angular momentum of the system ($\mathbf{J}$) can be assumed to be equal to the reactants orbital angular momentum ($\mathbf{l}$), as the modulus of $\mathbf{l}$ is much larger than that of the O_2 rotational angular momentum ($\mathbf{j}$). In these cases, we observe a clear partition of the orbital angular momentum ($\mathbf{l}$) between the final orbital ($\mathbf{l}'$) and NO rotational ($\mathbf{j}'$) angular momenta ($\mathbf{l} \rightarrow \mathbf{l}' + \mathbf{j}'$). The partition of $\mathbf{l}$ between $\mathbf{l}'$ and $\mathbf{j}'$ changes for the different PESs and collision energies. For example, at medium and high collision energies ($E_T = 0.25$, 0.5, and 1.0 eV) and for the 2 $^2A'$ PES, a clear equipartition exists, i.e., $\mathbf{l}/2 \rightarrow \mathbf{l}'$ and $\mathbf{l}/2 \rightarrow \mathbf{j}'$. In other cases, the angular momentum transformation is less evident and the $|\mathbf{j}'|/|\mathbf{l}|$ and $|\mathbf{l}'|/|\mathbf{l}|$ distributions are very broad.

To obtain a more complete description of the stereodynamics of the title reaction, we also examined the two-vector angular distributions $\mathbf{kk}'$, $\mathbf{kj}'$, $\mathbf{k}'\mathbf{j}'$, and $\mathbf{l}'\mathbf{j}'$, where $\mathbf{k}$ ($\mathbf{k}'$) is the initial (final) relative velocity vector. These properties are expressed in terms of the solid angle differential cross section [$d\sigma/d\Omega$, differential cross section (DCS) hereafter].

Figure 4 shows the global $\mathbf{kk}'$ distribution at different collision energies, as well as the contribution of the different PESs to the total DCS. At low E_T values the overall $\mathbf{kk}'$ angular distribution is predominantly backward [$\langle \mathbf{kk}' \rangle = 99.9°$ and the forward/backward (f/b) scattering ratio is equal to 0.63] (Table III). When E_T increases the backward scattering diminishes and the $\mathbf{kk}'$ distribution evolves to an essentially sideways distribution. Thus, at high collision energies ($E_T = 1.00$ eV) $\langle \mathbf{kk}' \rangle = 90.8°$ and $f/b = 1.00$. The loss of backward feature with E_T for the overall reaction arises from the particular behavior of each one of the PESs investigated.

In general, the 2 $^2A'$, 3 $^2A'$, and 2 $^2A''$ PESs present a clear backward distribution for all collision energies explored. However, this behavior becomes less noticeable as E_T rises. For example, in the case of the 2 $^2A'$ PES $\langle \mathbf{kk}' \rangle = 111.4°$ and $f/b = 0.35$ at 0.0388 eV, and $\langle \mathbf{kk}' \rangle = 95.2°$ and $f/b = 0.82$ at 1.00 eV. A decrease of backward character with E_T is known to occur for direct reaction pathways evolving through an energy barrier, as it is the case for the MEP of the 2 $^2A'$, 3 $^2A'$, and 2 $^2A''$ PESs. For such a situation the following expression was derived.[38]

TABLE III. $\langle \mathbf{kk}' \rangle$ and $\langle \mathbf{l}'\mathbf{j}' \rangle$ values for the four PESs involved in reaction (2).

E_T/eV	2 $^2A'$	3 $^2A'$	1 $^2A''$	2 $^2A''$	Global[a]
			$\langle \mathbf{kk}' \rangle$/°[b]		
0.0388	111.4		93.5		99.9
0.25	111.8	125.5	75.8		92.5
0.50	103.3	117.2	74.9	120.9	93.5
1.00	95.2	105.8	70.4	111.3	90.8
			f/b[b]		
0.0388	0.35		0.83		0.63
0.25	0.32	0.05	1.97		0.88
0.50	0.54	0.25	2.12	0.16	0.87
1.00	0.82	0.46	2.83	0.36	1.00
			$\langle \mathbf{l}'\mathbf{j}' \rangle$/°[b]		
0.0388	147.9		158.0		154.4
0.25	103.4	158.4	138.8		124.0
0.50	96.2	131.5	124.5	146.7	115.5
1.00	90.4	102.3	110.9	105.8	102.1
			p/ap[b]		
0.0388	0.040		0.0039		0.020
0.25	0.61	0.00010	0.070		0.25
0.50	0.89	0.10	0.19	0.0079	0.36
1.00	1.27	0.57	0.36	0.49	0.62

[a]The global values have been obtained using an analogous expression to the one reported in Table I for the calculation of the global average energy fractions.

[b]$\langle \mathbf{kk}' \rangle$ and $\langle \mathbf{l}'\mathbf{j}' \rangle$ stand, respectively, for the average $\mathbf{kk}'$ and $\mathbf{l}'\mathbf{j}'$ angles values derived from the DCS($\mathbf{kk}'$) and DCS($\mathbf{l}'\mathbf{j}'$) distributions; f/b is the ratio of products recoiled in the forward ($\mathbf{kk}' < 90°$) and backward ($\mathbf{kk}' > 90°$) hemispheres; p/ap is the ratio of products formed within the parallel ($\mathbf{l}'\mathbf{j}' < 90°$) and antiparallel ($\mathbf{l}'\mathbf{j}' > 90°$) $\mathbf{l}'\mathbf{j}'$ orientation regions.

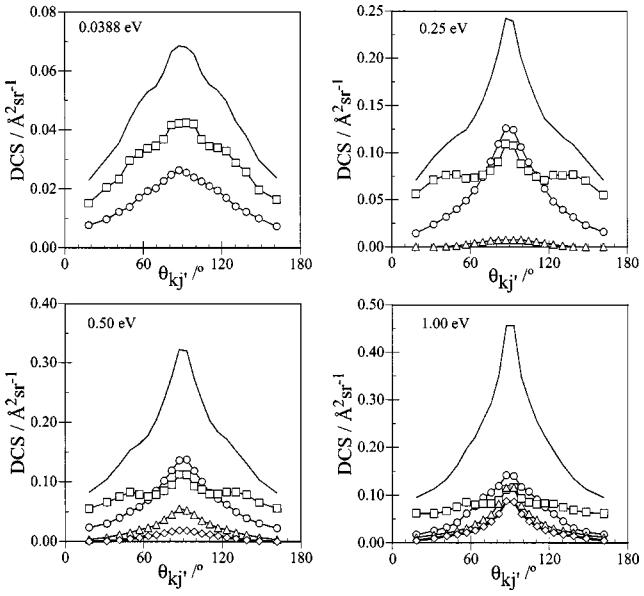

FIG. 5. DCS($\mathbf{kj}'$) at several collision energies for the (○) $2\,^2A'$ PES, (□) $1\,^2A''$ PES, (△) $3\,^2A'$ PES, (◇) $2\,^2A''$ PES, and (—) global.

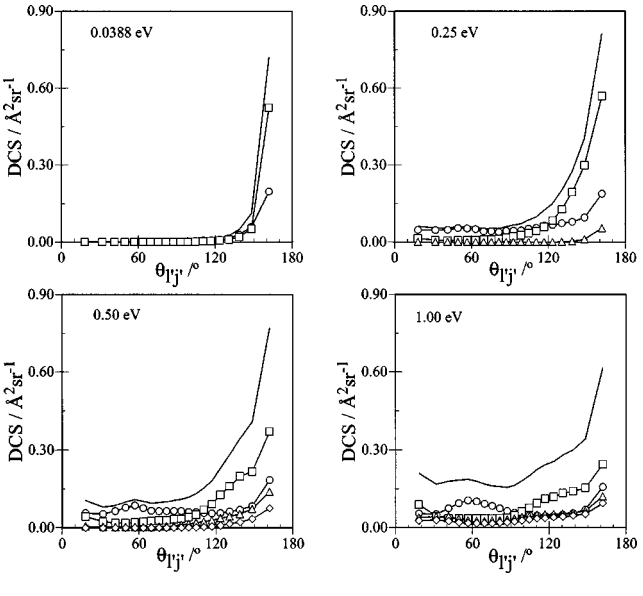

FIG. 6. DCS($\mathbf{l}'\mathbf{j}'$) at several collision energies for the (○) $2\,^2A'$ PES, (□) $1\,^2A''$ PES, (△) $3\,^2A'$ PES, (◇) $2\,^2A''$ PES, and (—) global.

$$\theta_{kk'}(b,E_T)=\lambda(b)/E_T. \tag{3}$$

In Eq. (3) $\lambda(b)$ is a function of the impact parameter and $\theta_{kk'}(b,E_T)$ is the scattering function that gives the $\mathbf{kk}'$ angle for fixed values of b and E_T. From this expression it comes out that more forward scattering is expected for a given value of b as E_T increases. Moreover, changes in the opacity function with E_T may also influence the scattering of products because a correlation between b and the $\mathbf{kk}'$ angle is expected. Thus, we found that the higher b is, the lower the $\mathbf{kk}'$ angle becomes for the $2\,^2A'$, $3\,^2A'$, and $2\,^2A''$ PESs. Therefore, the larger contribution to reactivity of high b values as E_T rises (see Fig. 2) also favors the loss of backward feature of the DCS($\mathbf{kk}'$) distribution when collision energy increases.

On the other hand, the DCS($\mathbf{kk}'$) distribution for the $1\,^2A''$ PES is not backward, but it presents a sideways feature for $E_T=0.0388$ eV that transforms to a forward feature as collision energy increases. Actually, $\langle \mathbf{kk}' \rangle = 93.5$ and 70.4° and the f/b ratio is equal to 0.83 and 2.83 for $E_T=0.0388$ and 1.0 eV, respectively. This behavior is due to the occurrence of two reaction mechanisms for the $1\,^2A''$ PES. The larger forward feature of the DCS($\mathbf{kk}'$) distributions corresponding to the two mechanisms as collision energy increases (due to the same reasons outlined above for the other PESs) and their different contribution to reactivity depending on E_T explain the behavior of the global DCS($\mathbf{kk}'$) function for the $1\,^2A''$ PES. This will be further discussed in Sec. III C.

The $\mathbf{kj}'$ DCS distributions for the global reaction and the four different PESs studied are symmetric around 90° (as they must be), where they exhibit a maximum (Fig. 5). The global DCS($\mathbf{kj}'$) becomes narrower as collision energy increases, which means that the tendency to a perpendicular $\mathbf{kj}'$ arrangement is more noticeable with E_T. This trend can also be inferred from the analysis of the product rotational alignment parameter $[A_0^{(2)} \equiv \langle 3\cos^2\theta - 1 \rangle$, with θ being the $\mathbf{kj}'$ angle in this case], whose limiting values correspond to a fully perpendicular $[A_0^{(2)}=-1]$ or parallel $[A_0^{(2)}=+2]$ $\mathbf{kj}'$ alignment. The value of this parameter for the overall reaction is equal to −0.26, −0.28, −0.32, and −0.38 for $E_T=0.0388$, 0.25, 0.50, and 1.0 eV, respectively. Thus, the higher the collision energy is, the closer $A_0^{(2)}$ is to the perpendicular limiting value. This situation is also observed for the $2\,^2A'$, $3\,^2A'$, and $2\,^2A''$ PESs, while the occurrence of two reaction mechanisms for the $1\,^2A''$ PES favors a less perpendicular $\mathbf{kj}'$ alignment trend as E_T increases. For $E_T=1.00$ eV, $A_0^{(2)}=-0.48$, −0.50, −0.56, and −0.14 for the $2\,^2A'$, $3\,^2A'$, $2\,^2A''$, and $1\,^2A''$ PESs, respectively.

With regard to the $\mathbf{l}'\mathbf{j}'$ DCS, the $\mathbf{l}'$ and $\mathbf{j}'$ vectors present a predominant antiparallel orientation at low collision energies, and when collision energy increases, this distribution tends to lose preference for the antiparallel orientation (Fig. 6). This behavior is found for both the global reaction and all the PESs investigated. For the global reaction $\langle \mathbf{l}'\mathbf{j}' \rangle = 154.4°$ and the parallel/antiparallel (p/ap) ratio is equal to 0.016 at $E_T=0.0388$ eV, while $\langle \mathbf{l}'\mathbf{j}' \rangle = 102.1°$ and $p/ap=0.62$ at $E_T=1.00$ eV. Nevertheless, the antiparallel orientation in general dominates within the range of E_T values explored.

The $\mathbf{k}'\mathbf{j}'$ DCS for the global reaction and all the PESs studied corresponds to a symmetric distribution, as it must be (Fig. 7). For $E_T=0.0388$ eV, the overall DCS($\mathbf{k}'\mathbf{j}'$) presents a maximum around 90° and preferential perpendicular alignment $[A_0^{(2)}=-0.81]$. As collision energy increases, the peak at 90° disappears and two new maxima at around 40° and 140° are observed. This results in a loss of $\mathbf{k}'\mathbf{j}'$ perpendicular alignment with E_T $[A_0^{(2)}=-0.26$, −0.11, and 0.07 for $E_T=0.25$, 0.5, and 1.0 eV, respectively]. This situation correlates with the behavior of the DCS($\mathbf{l}'\mathbf{j}'$) because antiparallel $\mathbf{l}'\mathbf{j}'$ orientation leads to perpendicular $\mathbf{k}'\mathbf{j}'$ alignment. As mentioned above, the antiparallel $\mathbf{l}'\mathbf{j}'$ orientation diminishes with E_T and so does the perpendicular $\mathbf{k}'\mathbf{j}'$ alignment. Such a behavior is specially accentuated for the $2\,^2A'$,

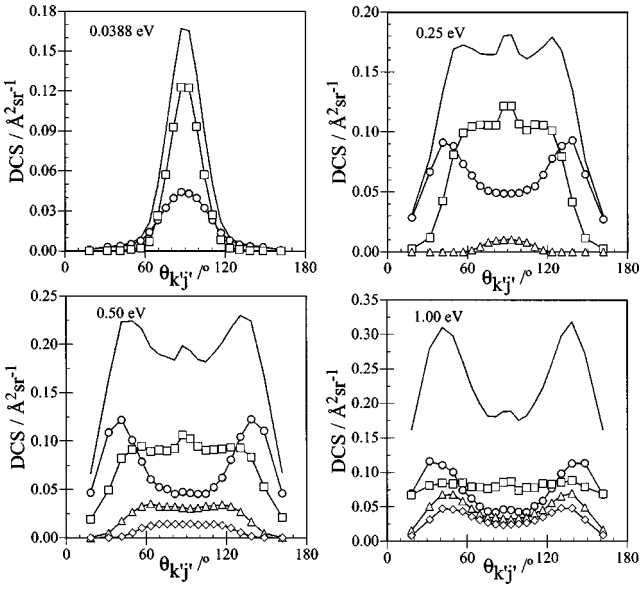

FIG. 7. DCS($\mathbf{k}'\mathbf{j}'$) at several collision energies for the (○) 2 $^2A'$ PES, (□) 1 $^2A''$ PES, (△) 3 $^2A'$ PES, (◇) 2 $^2A''$ PES, and (—) global.

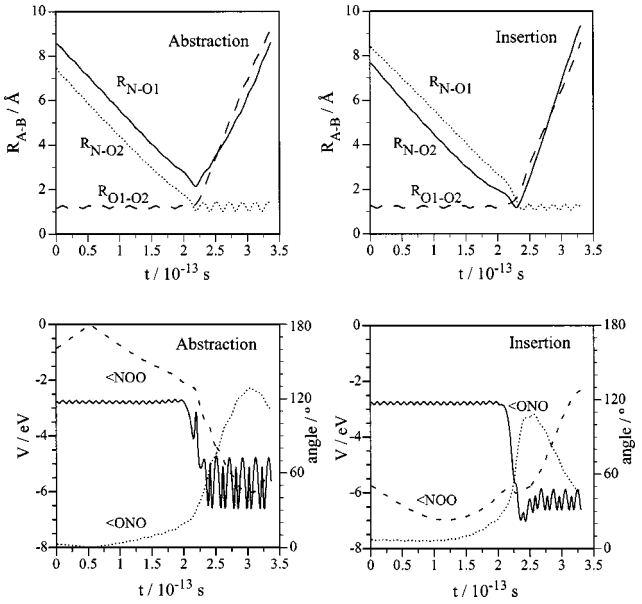

FIG. 8. Typical reactive trajectories corresponding to the abstraction and insertion microscopic mechanisms for the 1 $^2A''$ PES, plotted in terms of the internuclear distances, angles, and potential energy.

3 $^2A'$, and 2 $^2A''$ PESs, which results in pronounced minima at 90° in the DCS($\mathbf{k}'\mathbf{j}'$) for high E_T values. On the other hand, the loss of antiparallel $\mathbf{l}'\mathbf{j}'$ orientation as the collision energy increases is less clear for the 1 $^2A''$ PES, which explains that the DCS($\mathbf{k}'\mathbf{j}'$) for high collision energies still preserves the peak at 90°, although it broadens with E_T.

C. Reaction mode

We investigated the microscopic reaction mechanisms (reaction modes) taking place on the PESs studied. On the 2 $^2A'$, 3 $^2A'$, and 2 $^2A''$ PESs all reactive trajectories analyzed evolve through an abstraction mechanism of direct type via a saddle point of bent geometry. In fact, the dynamic properties described for these three PESs in the previous sections are similar to the ones expected for a rebound-type reaction mode. Namely, reactivity is favored for low b values yielding backward scattering of products.

However, the 1 $^2A''$ PES presents an additional mode of reaction (insertion). As we have already explained, this PES has two saddle points with low enough energy barriers to allow reaction to occur at low temperatures. The first saddle point has C_s symmetry and connects reactants [N(^2D) + O_2] and products [O(^3P)+NO] of reaction (2) through an abstraction pathway, in a similar way as in the 2 $^2A'$, 3 $^2A'$, and 2 $^2A''$ PESs. The second saddle point, however, presents C_{2v} symmetry and connects reactants with a NO_2 minimum. From this minimum, after distortion of the C_{2v} symmetry, it is possible to reach products without surmounting any barrier. Therefore, the saddle point of C_{2v} symmetry gives rise to an insertion mechanism, in which trajectories are influenced by the presence of the NO_2 minimum that is located 23.62 kcal mol^{-1} below products. Reactive trajectories on the 1 $^2A''$ PES could evolve through any of these two mechanisms, then leading to different dynamic properties.

Figure 8 shows a schematic representation of two examples of both types of reactive trajectories (abstraction and insertion). For the reactive trajectories corresponding to the insertion mechanism, there is a point where the N–O1 and N–O2 distances have small and similar values. Then the geometry of the system is close to that of the NO_2 minimum and, consequently, the value of the potential energy is below the energy of products. Despite the exploration of this minimum, we did not observe the formation of collision complexes for this kind of trajectories. This is usually explained on the basis of the small depth of the minimum with respect to products, the high energy content of the system when it reaches this region of the PES and the low number of degrees of freedom involved. All these characteristics prevent the formation of collision complexes.

With regard to the abstraction mechanism, there is an oxygen atom (O1 in Fig. 8) that remains at a long distance ($\geqslant$2.0 Å) from the attacking nitrogen atom during the trajectory, while the potential energy is always kept higher than the energy of products. Moreover, at the closest approach distance between the three atoms, the trajectories evolving through abstraction present a NOO angle of about 120° (corresponding to the angle of the abstraction saddle point), while the trajectories evolving through insertion show a much smaller NOO angle, corresponding to the insertion saddle point. This indicates that the trajectories exhibiting an abstraction mechanism do not explore the region of the PES where the NO_2 minimum is located.

Table IV shows the percentage of reactive trajectories that evolve through each type of microscopic mechanism on the 1 $^2A''$ PES as a function of collision energy. At low collision energies (0.0388 eV) the number of reactive trajectories occurring via insertion is only about 18% of the total ones. This fact is due to the different values of the energy barriers for both mechanisms. The saddle point of C_s symmetry that allows the abstraction reaction mode to take place

TABLE IV. Yield (in %) of the two microscopic mechanisms of the $1\,^2A''$ PES.

E_T/eV	Abstraction	Insertion
0.0388	81.4	18.6
0.25	56.1	43.9
0.50	52.6	47.4
1.00	47.2	52.8

presents an energetic requirement of $0.21\,\mathrm{kcal\,mol^{-1}}$, whereas in the case of the saddle point of C_{2v} symmetry associated to the insertion mode the energy barrier is $1.43\,\mathrm{kcal\,mol^{-1}}$. The contribution of the insertion mechanism increases with E_T, the insertion and abstraction mechanisms having similar yields at $E_T=0.5$ and 1.0 eV.

The cross section, average fraction of energies, NO vibrational distribution and DCS($\mathbf{kk}'$) for the $1\,^2A''$ PES, as a function of the reaction mode, are given in Fig. 9 for some selected conditions. Concerning the scalar properties, we observed some differences in both mechanisms. While abstraction yields excited NO vibrational distributions similar to the ones obtained for the $2\,^2A'$, $3\,^2A'$, and $2\,^2A''$ PESs, the insertion mechanism results in less excited distributions peaked at low v' (at $E_T=0.5$ eV, $v'_{\max}=1$) [Fig. 9(c)]. This might be due to the presence of the NO_2 minimum in the insertion pathway, which may allow for a more efficient equipartition of the available energy among translational, vibrational, and rotational energy. The different behavior of both mechanisms leads to a bimodal NO vibrational distribution for the $1\,^2A''$ PES. This bimodal behavior is smoothed out at high collision energies, as the inverted vibrational distribution arising from the abstraction mechanism is less excited.

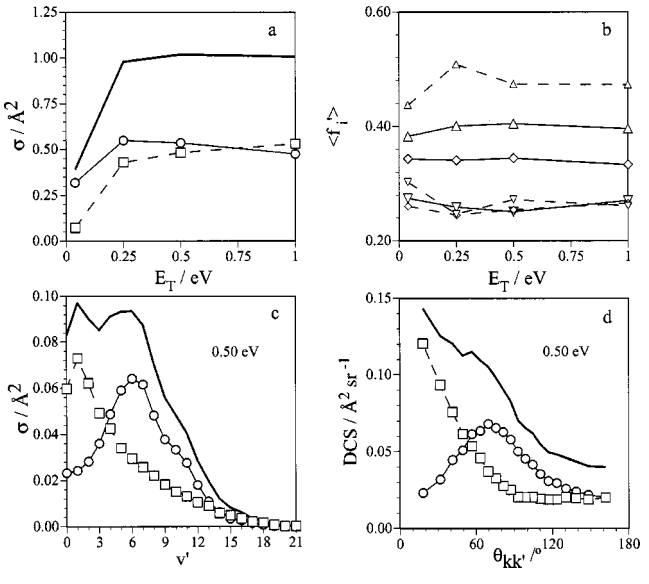

FIG. 9. (a) Cross section (—) for the $1\,^2A''$ PES and for the two reaction mechanisms of this PES: (○) abstraction and (□) insertion; (b) average fractions of energy in the $1\,^2A''$ PES for the two mechanisms: (--△--) translation, (--▽--) rotation, and (--◇--) vibration for insertion, and (-△-) translation, (-▽-) rotation, and (-◇-) vibration for abstraction; (c) vibrational distribution of NO (—) for the $1\,^2A''$ PES and for the two reaction mechanisms of this PES: (○) abstraction and (□) insertion; (d) $\mathbf{kk}'$ angular distribution (—) for the $1\,^2A''$ PES and for the two reaction mechanisms: (○) abstraction and (□) insertion.

The average fractions of energy in products are also different for both mechanisms [Fig. 9(b)]. On the one hand, we observed that the average fractions of vibrational, rotational and translational energies are rather constant with collision energy for both mechanisms. As refers to $\langle f'_R\rangle$ there are no important differences between the two mechanisms. Instead, $\langle f'_V\rangle$ and $\langle f'_T\rangle$ present different features for insertion and abstraction. $\langle f'_V\rangle$ is higher for abstraction than for insertion (in consistency with what we have observed before: abstraction yields more excited vibrational distributions than insertion). Moreover, reactive trajectories that evolve through the insertion mechanism present higher values of $\langle f'_T\rangle$.

Regarding to the two-vector properties, the most important difference between the two mechanisms refers to the $\mathbf{kk}'$ angular distribution. The insertion mechanism yields in all cases a clearly forward scattering of products, whereas the abstraction mechanism is backward at low collision energy ($E_T=0.0388$ eV) and becomes sideways at medium and high energies, as it occurs for the $\mathbf{kk}'$ distributions of the $2\,^2A'$, $3\,^2A'$, and $2\,^2A''$ PESs. For the $\mathbf{l}'\mathbf{j}'$, $\mathbf{kj}'$, and $\mathbf{k}'\mathbf{j}'$ angular distributions, there are no important differences between both mechanisms.

IV. SUMMARY AND CONCLUSIONS

A study of the collision energy effects on the dynamics of the $N(^2D)+O_2\rightarrow O(^3P)+NO$ reaction was performed using the QCT method on the main four analytical potential energy surfaces recently derived by us, and neglecting nonadiabatic couplings between them. These PESs correspond to the main surfaces of the system. Scalar and two-vector properties of the reaction were analyzed in terms of the collision energy, paying particular attention to the following E_T values: 0.0388, 0.25, 0.50, and 1.00 eV.

The cross section of the reaction increases with E_T, due to the increase of the reaction probability in the four PESs studied. The available energy is mainly channeled into vibrational and translational energy of products. The vibrational distribution of NO is inverted, though it becomes less excited as E_T increases.

Concerning the two-vector correlations (expressed as DCSs), the $\mathbf{kk}'$ angular distribution is backward at low collision energy and at higher E_T values it becomes sideways. In addition, a predominant antiparallel orientation of the $\mathbf{l}'$ and $\mathbf{j}'$ vectors is observed at low collision energies, though this orientation preference is smoothed out when E_T increases.

Finally, we investigated the microscopic reaction mechanism occurring on the four PESs considered. For the $2\,^2A'$, $3\,^2A'$, and $2\,^2A''$ PESs only an abstraction mechanism is observed. However, for the $1\,^2A''$ PES both an abstraction mechanism and an insertion mechanism can occur leading to different dynamic properties. Nevertheless, both mechanisms are of direct type.

Further work on this reaction studying the influence of the internal excitation of reactants on the dynamics is in progress in our group.

ACKNOWLEDGMENTS

This work was supported by the ''Dirección General de Enseñanza Superior'' of the Spanish Ministry of Education and Culture through the DGES project Ref. No. PB98-1209-C02-01, and also by the ''Dirección General de Investigación'' of the Spanish Ministry of Science and Technology through the DGI projects Refs. BQU2002-04269-C02-02 and BQU2002-03351. Financial support from the ''Generalitat'' (Autonomous Government of Catalonia) (Ref. 2001SGR 00041) and the European Union (INTAS Ref. 99-00701) is also acknowledged. I.M. also thanks the ''Generalitat'' for a ''Beca de Formació d'Investigadors'' (Predoctoral Research Grant). The authors are also grateful to the ''Center de Computació i Comunicacions de Catalunya [C^4 (CESCA/CEPBA)]'' for providing a part of the computer time.

[1] M. González, I. Miquel, and R. Sayós, Chem. Phys. Lett. **335**, 339 (2001), and references therein.
[2] M. W. Chase, Jr., C. A. Davies, J. R. Downey, Jr., D. J. Frurip, R. A. McDonald, and A. N. Syverud, J. Phys. Chem. Ref. Data Suppl. **1**, 14 (1985).
[3] S. Baskin, and J. A. Stanner, *Atomic Energy Levels and Grotrian Diagrams 1* (North-Holland, Amsterdam, 1975), Vol. 1.
[4] F. Kaufman, ''Atmospheric reactions involving neutral constituents: An evaluation,'' presented at the American Geophysical Union Meeting, San Francisco, CA, December, 1968.
[5] G. Black, T. G. Slanger, G. A. St. John, and R. A. Young, J. Chem. Phys. **51**, 116 (1969).
[6] C. L. Lin and F. Kaufman, J. Chem. Phys. **55**, 3760 (1971).
[7] T. G. Slanger, B. J. Wood, and G. Black, J. Geophys. Res. **76**, 8430 (1971).
[8] D. Husain, L. J. Kirsch, and J. R. Wiesenfeld, Faraday Discuss. Chem. Soc. **53**, 201 (1972).
[9] D. Husain, S. K. Mitra, and A. N. Young, J. Chem. Soc., Faraday Trans. 2 **10**, 1721 (1974).
[10] J. E. Davenport, T. G. Slanger, and G. Black, J. Geophys. Res. **81**, 12 (1976).
[11] M. P. Iannuzzi and F. Kaufman, J. Chem. Phys. **73**, 4701 (1980).
[12] B. Fell, I. V. Rivas, and D. L. McFadden, J. Phys. Chem. **85**, 224 (1981).
[13] L. G. Piper, M. E. Donahue, and W. T. Rawlins, J. Phys. Chem. **91**, 3883 (1987).
[14] P. D. Whitefield and F. E. Hovis, Chem. Phys. Lett. **135**, 454 (1987).
[15] J. Herron, J. Phys. Chem. Ref. Data **28**, 1453 (1999).
[16] Y. Shihira, T. Suzuki, S. Unayuma, H. Umemoto, and S. Tsunashima, J. Chem. Soc., Faraday Trans. **90**, 549 (1994).
[17] L. E. Jusinski, G. Black, and T. G. Slanger, J. Phys. Chem. **92**, 5977 (1988).
[18] W. T. Rawlins, M. E. Fraser, and S. M. Miller, J. Phys. Chem. **93**, 1097 (1989).
[19] M. González, I. Miquel, and R. Sayós, J. Chem. Phys. **115**, 2530 (2001).
[20] M. González, I. Miquel, and R. Sayós, J. Chem. Phys. **115**, 8838 (2001).
[21] M. González, I. Miquel, and R. Sayós, Chem. Phys. Lett. **360**, 521 (2002).
[22] I. Miquel, R. Sayós, and M. González (unpublished).
[23] I. Miquel, M. González, R. Sayós, G. G. Balint-Kurti, S. K. Gray, and E. M. Goldfield, J. Chem. Phys. **118**, 3111 (2003).
[24] M. Braunstein and J. W. Duff, J. Chem. Phys. **113**, 7406 (2000).
[25] B. O. Roos, P. R. Taylor, and P. E. M. Siegbahn, Chem. Phys. **48**, 157 (1980).
[26] B. O. Roos, Adv. Chem. Phys. **69**, 399 (1987).
[27] T. H. Dunning, Jr., J. Chem. Phys. **90**, 1007 (1989).
[28] K. Andersson, Theor. Chim. Acta **91**, 31 (1995).
[29] J. N. Murrell, S. Carter, S. C. Farantos, P. Huxley, and A. J. C. Varandas, *Molecular Potential Energy Surfaces* (Wiley, New York, 1984).
[30] L. M. Raff and D. L. Thompson, in *Theory of Chemical Reaction Dynamics*, edited by M. Baer (CRC, Boca Raton, 1985), Vol. III.
[31] H. R. Mayne, Int. Rev. Phys. Chem. **10**, 107 (1991).
[32] R. Sayós *et al.* TRIQCT (unpublished program).
[33] M. González, J. D. Sierra, R. Francia, and R. Sayós, J. Phys. Chem. A **101**, 7513 (1997).
[34] M. González, D. Troya, M. P. Puyuelo, R. Sayós, and P. A. Enríquez, Chem. Phys. Lett. **300**, 603 (1999).
[35] M. González, R. Valero, and R. Sayós, J. Chem. Phys. **113**, 10983 (2000).
[36] R. Sayós, J. Hernando, M. P. Puyuelo, P. A. Enríquez, and M. González, Chem. Phys. Lett. **341**, 608 (2001).
[37] R. Sayós, J. Hernando, M. P. Puyuelo, P. A. Enríquez, and M. González, Phys. Chem. Chem. Phys. **4**, 288 (2002).
[38] R. D. Levine and R. B. Bernstein, *Molecular Reaction Dynamics* (Oxford University Press, New York, 1987).